NUMERICAL AND EXPERIMENTAL STUDY OF SHOCK/TURBULENT FLOW INTERACTION – A CODE VALIDATION TEST

Mohammad Ali Jinnah[1] and Kazuyoshi Takayama[2]

[1]*MCE Department, Islamic University of Technology, Board Bazar, Gazipur-1704*
[2]*Multidisciplinary Shock Wave Research Center, Tohoku University,*
2-1-1 katahira, Aoba-ku, Sendai 980-8577, Japan
E-mail: [1]jinnah@iut-dhaka.edu

ABSTRACT

A numerical code has been developed to solve the shock/turbulence interaction using grid adaptation technique. For the code validation test, shock wave propagations through nozzle are studied experimentally and numerically for the incident shock Mach number 1.60. The experimental photographs, taken by double exposure holographic interferometry, are used for the code validation test and a comparison is conducted between the experimental photographs and the numerical images. The shock wave propagation through a nozzle of small throat area is selected where laminar flow structures, transition phenomena, flow separation line as well asviscous boundary layer separation, wave propagation through the throat of the nozzle and shock wave reflection from converging area of the nozzle are observed numerically. The numerical results agree well with the experiment results. The numerical code is used to solve the two-dimensional Navier-Stokes equations with k-ε turbulence model for the solution of the shock wave propagation through the nozzle and this code later has been extended to develop a three-dimensional code. The three-dimensional code is used to solve the shock or turbulence interaction for a compressible fluid. A grid convergence study has been performed to validate the interaction results. The Navier-Stokes Simulation (NS) results for the shock wave interaction with turbulence are compared with the Navier-Stokes Simulation (NS) results with k-ε turbulence model and the comparison results are good enough to validate the present simulation works.

Keywords: *Navier-Stokes Equations, Shock or turbulence Interaction, Shock Wave, Turbulent Flow, Turbulence Model*

1.0 INTRODUCTION

The investigation on shock or turbulence interaction is an important feature due to its complexity to determine the characteristics of the turbulence by experimentally and numerically. Experimental realization of a homogeneous and isotropic turbulent flow interacting with a normal shock wave in the laboratory is a difficult task due to generation of compressible and isotropic turbulent flow and the generation of a normal shock wave interacting with flow. Experimentally and numerically many researchers got many results on shock or turbulence interaction. The outcomes of the interactions of shock wave with homogeneous and isotropic turbulence are the amplification of longitudinal velocity fluctuation, the amplification of turbulent kinetic energy level and substantial changes in length scales. The selection of homogeneous and isotropic turbulent field interactions is the easier phenomena than the other types of turbulent field like turbulent boundary layer interactions, turbulent wake-shock interaction. Turbulence amplification through shock wave interactions is a direct effect of the Rankine-Hugoniot relations. The study of the interaction of turbulence with a shock wave is of fundamental importance in engineering applications. For designing aero-mechanism system such as transport aircraft of supersonic and hypersonic speed, the shock wave and turbulence interaction effects are the important phenomena. The shock or turbulence interaction effects are generally seen in aero-mechanism system and in combustion process as well as high-speed rotor flows.

The study of the interaction of turbulence with a shock wave began in the early 1950s with the development of linear theories. Ribner [1-3] investigated how a shock wave is perturbed by an impinging single shear wave. The theory, later on called Ribner's theory, is, in fact, mostly based on the mode theory developed by Kovasznay [4] and extended to the shock problem by focusing mainly on the acoustic field generated by the interaction with the shock wave. Using his general theory of aerodynamic sound generation, Lighthill [5] estimated the acoustic energy scattered from the interaction of turbulence with a shock wave. Analytical studies of shock-turbulence interaction (Ribner [1]; Moore [6]; Kerrebrock [7]) were developed using a linearised description of the interaction of plane disturbances interacting with a shock wave.

These disturbances were represented as waves of vorticity, entropy, or sound (Kovasznay [4]) and these disturbances interacting with the shock wave generates the fluctuations downstream of the shock wave. Ribner [1] investigated the passage of a single vorticity wave through a plane shock and its modification, with simultaneous generation of a sound wave in a reference frame fixed on the shock wave.

This analysis was later extended to study turbulence amplification due to a shock wave (Ribner [2]), the flux of acoustic energy emanating from the downstream side of the shock (Ribner [3]), and the one-dimensional power spectra of various fluctuations downstream of the shock (Ribner [8]). Moore [6] analysed the flow field produced by oblique impingement of weak plane disturbances on a normal shock wave in a reference frame fixed on the mean upstream flow. Anyiwo et al [9] revisited the linear analysis to identify primary mechanisms of turbulence enhancement – amplification of the vorticity mode, generation of acoustic and entropy modes from the interaction, and turbulence 'pumping' by shock oscillations.

The shock or turbulence interaction considerably modifies the fluid field by vorticity and entropy production and transport. Experimental evidence from shock wave/boundary layer interaction indicates amplification in Reynolds stresses and turbulence intensities across the shock wave. The physics, however, of the phenomena associated with this amplification is not well understood. The first attempt to predict such turbulence amplification across the shock is attributed to Ribner [1]. His predictions were verified by experiments conducted by Sekundov [10] and Donsanjh et al [11]. Several analytical and numerical studies of this phenomenon show very similar turbulence enhancement.

Chu et al [12] indicated that there are three fluctuating modes, which are coupled and are responsible for the turbulence amplification. Acoustic (fluctuating pressure and irrotational velocity mode), turbulence (fluctuating vorticity mode) and entropy (fluctuating temperature mode) are the three fluctuating modes which are nonlinearly coupled and the Rankine-Hugoniot jump conditions across the shock indicate that when any one of the three fluctuation modes is transferred across a shock wave, it not only generates the other two fluctuation modes, but it may itself also be considerably amplified.

Many researcher conducted experiments on the interaction of turbulent boundary layers with an oblique shock wave. A general finding from the experiments is that Reynolds shear stress and turbulence intensities are amplified across the shock wave. The interaction of an oblique shock wave with a turbulent boundary layer involves several complex phenomena like, unsteady flow separation in the interaction region, oscillation of the shock wave in the longitudinal direction, streamline curvature, and inhomogeneity effects due to walls. Due to above complications, it has been difficult to determine through these experiments the effect of shock wave on turbulence.

Experiments on the interaction between the shock wave and grid-generated turbulence, were conducted by Debreve et al [13] and they measured velocity and temperature spectra upstream and downstream of the shock wave and concluded that turbulent fluctuations are amplified and Taylor micro scales increase during the interaction. Jacquin et al [14] investigated the interactions of a normal shock wave with grid-generated turbulence and a turbulent jet and they observed that turbulence amplification was not significant for the grid-generated turbulence and that the decay of turbulent kinetic energy was accelerated downstream of the shock wave.

Their experiments treated the interaction of a shock with quasi-incompressible turbulence where fluctuations in pressure and density are not significant. They have observed that the data obtained from grid-generated turbulence are not sufficient to characterise the turbulence properly. They have analysed the flow by means of laser Doppler velocimetry. The obtained supersonic flow is shocked by means of a second throat creating a pure normal shock wave or free turbulence interaction. On other hand, Debreve et al [13] obtain a quasihomogeneous turbulence by generating perturbations in the settling chamber of a supersonic wind tunnel at Mach 2.3.

They show that, after the expansion in the nozzle, the turbulent field becomes strongly non-isotropic and that the turbulence level is drastically decreased leading to experimental difficulties. Debieve et al [15] analysed the evolution of turbulence through a shock, and separated the effects of the specific turbulent sources from the effects of the mean motion-convection and production. Their prediction of the longitudinal velocity fluctuation was in good agreement with the experimental results. An experimental work was performed on the interaction of weak shocks (M_s = 1.007, 1.03 and 1.1) with a random medium of density in homogeneity by Hesselink et al [16].

They observed that the pressure histories of the distorted shock waves were both peaked and rounded and explained these features in terms of the focusing or defocusing of the shock front due to in homogeneity of the medium. The Richtmyer- Meshkov instability (Richtmyer [17] and Meshkov [18]) provides an important example of the interaction of a shock wave and a material interface. This instability is observed when a shock wave passes normally through a perturbed interface between two fluids of different densities. Experiments of such an instability show that a single shock wave will cause the perturbation's amplitude to grow linearly with time.

However, interaction of the perturbation with a second shock stimulates the growth of the mixing zone between the gases. One interpretation of the experiments is that mixing is enhanced, that is the mixing zone between the two fluids grows, by the interaction of the shock wave with the turbulent or random flow field left behind the first shock wave.

In the present validation test of 2D code for the solution of Navier-Stokes equations, shock wave propagations through nozzle are studied experimentally and numerically. The shock wave propagation through a nozzle of small throat area is selected where laminar flow structures, transition phenomena, flow separation line as well as viscous boundary layer separation, wave propagation through the throat of the nozzle and shock wave reflection from converging area of the nozzle are observed numerically.

A good numerical simulation for nozzle flow depends on the throat area and the converging or diverging angle of the nozzle and the strength of the shock wave propagate through the throat of the nozzle. After the validation test of the 2D code, the extended code for the solution of three-dimensional Navier-Stokes equations with k-ε turbulence model is developed to solve almost all types of shock or turbulence interaction problems. For the better solution of the flow field, the improved three-dimensional grid adaptation technique is applied in these computations.

2.0 NUMERICAL METHOD

The three-dimensional unsteady, compressible, Reynolds-averaged Navier-stokes equations with k-ε turbulence model are solved by shock capturing method. Without external forces and heat sources, the conservative form of non-dimensionalised governing equation in three-dimensional Cartesian coordinate system is:

$$\frac{(\partial Q)}{\partial t} + \frac{\partial (F - Fv)}{\partial x} + \frac{\partial (G - Gv)}{\partial y} + \frac{\partial (H - Hv)}{\partial z} = S(Q) \quad (1)$$

where, $Q = [\rho, \rho u, \rho v, \rho w, e, \rho k, \rho \varepsilon]$,
$F = [\rho u, \rho u^2, \rho uv, \rho uw, u(e + p), \rho uk, \rho u \varepsilon]$,

$$G = [\rho v, \rho uv, \rho v^2, \rho vw, v(e+p), \rho vk, \rho v\varepsilon],$$
$$H = [\rho w, \rho uw, \rho vw, \rho w^2, w(e+p), \rho wk, \rho w\varepsilon]$$

and,

$$Fv = [0, \tau_{xx}, \tau_{xy}, \tau_{xz}, u\tau_{xx} + v\tau_{xy} + w\tau_{xz} - q_x, k_x, \varepsilon_x],$$
$$Gv = [0, \tau_{xy}, \tau_{yy}, \tau_{yz}, u\tau_{xy} + v\tau_{yy} + w\tau_{yz} - q_y, k_y, \varepsilon_y],$$
$$Hv = [0, \tau_{xz}, \tau_{yz}, \tau_{zz}, u\tau_{xz} + v\tau_{yz} + w\tau_{zz} - q_z, k_z, \varepsilon_z]$$

Here Q is the vector of conservative variables which contains mass, momentum and energy. All variables are calculated in per unit volume. ρ is taken as the mass per unit volume. Three momentum terms in three-dimensional Cartesian coordinates system are $\rho u, \rho v$ and ρw per unit volume. Total energy, e, turbulent kinetic energy, ρk and turbulent dissipative energy, $\rho \varepsilon$ are the energy terms per unit volume in these computations. F, G and H are the three inviscid flux vectors in X-, Y-, and Z-axis respectively. Similarly Fv, Gv and Hv are the three viscous flux vectors in X-, Y-, and Z-axis respectively. Each flux vectors contain mass flux, momentum flux and energy flux. ρu is the mass flux and ρu^2, ρuv, ρuw are the momentum flux and $u(e+p)$, ρuk, $\rho u\varepsilon$ are the energy flux in the X-axis. Similarly ρv is the mass flux and ρuv, ρv^2, ρvw are the momentum flux and $v(e+p)$, ρvk, $\rho v\varepsilon$ are the energy flux in the Y-axis and ρw is the mass flux and ρwu, ρvw, ρw^2 are the momentum flux and $w(e+p)$, ρwk, $\rho w\varepsilon$ are the energy flux in the Z-axis. Also ρ is the fluid density and u, v and w are velocity components in each direction of Cartesian coordinates. While e is the total energy per unit volume, pressure p can be expressed by the following state equation for ideal gas

$$p = (\gamma - 1)[e - \frac{1}{2}\rho(u^2 + v^2 + w^2)] \tag{2}$$

where γ is the ratio of specific heats. From the relationship between stress and strain and assumption of stokes, non-dimensional stress components are as follows:

$$\tau_{xx} = \frac{\mu}{Re}\frac{2}{3}\left(2\cdot\frac{\partial u}{\partial x} - \frac{\partial v}{\partial y} - \frac{\partial w}{\partial z}\right), \tau_{yy} = \frac{\mu}{Re}\frac{2}{3}\left(2\cdot\frac{\partial v}{\partial y} - \frac{\partial w}{\partial z} - \frac{\partial u}{\partial x}\right), \tau_{zz} = \frac{\mu}{Re}\frac{2}{3}\left(2\cdot\frac{\partial w}{\partial z} - \frac{\partial u}{\partial x} - \frac{\partial y}{\partial y}\right).$$

$$\tau_{xx} = \frac{\mu}{Re}\left(\frac{\partial v}{\partial x} - \frac{\partial u}{\partial y}\right), \tau_{yz} = \frac{\mu}{Re}\left(\frac{\partial w}{\partial y} - \frac{\partial v}{\partial z}\right), \tau_{zx} = \frac{\mu}{Re}\left(\frac{\partial u}{\partial z} + \frac{\partial w}{\partial x}\right).$$

$$k_x = \frac{1}{Re}\left(\mu_l + \frac{\mu_t}{\sigma_k}\right)\frac{\partial k}{\partial x}, \quad \varepsilon_x = \frac{1}{Re}\left(\mu_l + \frac{\mu_t}{\sigma_k}\right)\frac{\partial \varepsilon}{\partial x}$$

$$k_y = \frac{1}{Re}\left(\mu_l + \frac{\mu_t}{\sigma_k}\right)\frac{\partial k}{\partial y}, \quad \varepsilon_y = \frac{1}{Re}\left(\mu_l + \frac{\mu_t}{\sigma_k}\right)\frac{\partial \varepsilon}{\partial y}$$

$$k_z = \frac{1}{Re}\left(\mu_l + \frac{\mu_t}{\sigma_k}\right)\frac{\partial k}{\partial z}, \quad \varepsilon_z = \frac{1}{Re}\left(\mu_l + \frac{\mu_t}{\sigma_k}\right)\frac{\partial \varepsilon}{\partial z}$$

The expression of laminar viscosity is $\mu_l/\mu_o = c_v(T/T_o)1.5$ where μ_o is the laminar viscosity at the ambient temperature (T_o) and the coefficient, c_v depends on the temperature and the ambient gas. The total viscosity $\mu = \mu_l + \mu_t$ where μ_t is the turbulent eddy viscosity and the expression of turbulent eddy viscosity,

$$\mu_t = c_\mu \rho \frac{k^2}{\varepsilon} \tag{3}$$

The element of heat flux vectors are expressed by Fourier law of heat conduction as

$$q_x = \frac{kc}{Re}\frac{\partial T}{cx}, \quad q_y = \frac{kc}{Re}\frac{\partial T}{cy}, \quad q_z = \frac{kc}{Re}\frac{\partial T}{cz}$$

where T, is the temperature, k_c is the thermal conductivity and it expresses by $k_c = k_l + k_t$. The expression of the thermal conductivity of the laminar part is $k_l/k_o = ck(T/T_o)1.5$ where k_o is the

thermal conductivity at the ambient temperature and the value of the coefficient, c_k depends on the temperature and the ambient gas. The expression of the thermal conductivity of the turbulent part is $k_t = c_{tk}\frac{\mu_t}{Pr}$, where the value of the coefficient, c_{tk} depends on the temperature and the ambient gas and Pr is the Prandtl number based on characteristic values. The Reynolds number of the flow is defined by Re = $(\rho_c u_c l_c/\mu_o)$ where ρ_c, u_c, l_c and μ_o are respectively a characteristic density, a characteristic velocity, a characteristic length and the viscosity of the fluid.

The source term $S(Q)$ of the k-ε turbulence model is written by

$$S(Q) = [0, 0, 0, 0, 0, P_k - \rho\varepsilon - D_k, (c_{\varepsilon 1}.P_k - c_{\varepsilon 2}.\rho\varepsilon)\frac{\varepsilon}{k}] \tag{4}$$

where the production term P_k, which is the three-dimensional formulation, developed from the two-dimensional formulation of Kunz et al. (1992), is given in Cartesian coordinates as

$$P_k = \{2\mu_t\frac{\partial u}{\partial x} - \frac{2}{3}[\rho k + \mu_t\left(\frac{\partial u}{\partial x} + \frac{\partial v}{\partial y} + \frac{\partial w}{\partial z}\right)]\}\frac{\partial u}{\partial x} + \{2\mu_t\frac{\partial v}{\partial y} - \frac{2}{3}[\rho k + \mu_t\left(\frac{\partial u}{\partial x} + \frac{\partial v}{\partial y} + \frac{\partial w}{\partial z}\right)]\}$$

$$\frac{\partial v}{\partial y} + \{2\mu_t\frac{\partial w}{\partial z} - \frac{2}{3}[\rho k + \mu_t\left(\frac{\partial u}{\partial x} + \frac{\partial v}{\partial y} + \frac{\partial w}{\partial z}\right)]\} + \mu_t\left(\frac{\partial u}{\partial y} + \frac{\partial v}{\partial x}\right)^2 + \mu_t\left(\frac{\partial w}{\partial y} + \frac{\partial y}{\partial z}\right)^2 \tag{5}$$

and the destruction term D_k is given as $D_k = \frac{2\rho}{\gamma T}k\varepsilon$

The mass average turbulent kinetic energy and homogeneous component of turbulent kinetic energy dissipation rate are defined by as $k = \frac{1}{2}c_t^2(u^2 + v^2 + w^2)$ and $\varepsilon\ c_m\ k^2\ \frac{Re}{100}$ (6)

The various constants in the k-ε turbulence model are listed as follows:

$$c_\mu = 0.09, c_t = 0.03, c_m = 0.09, c_{\varepsilon 1} = 1.45, c_{\varepsilon 2} = 1.92, \sigma_k = 1.00, \sigma_\varepsilon = 1.30 \tag{7}$$

3.0 NUMERICAL DISCRETISATION AND GRID ADAPTATION

The governing equations described above for compressible viscous flow are discretised by the finite volume method. A second order, upwind Godunov scheme of Flux vector splitting method is used to discretise the inviscid flux terms and MUSCL-Hancock scheme is used for interpolation of variables. Central differencing scheme is used in discretising the viscous flux terms. HLL Reimann solver is used for shock capturing in the flow. Two equations for k-ε turbulence model are used to determine the dissipation of turbulent kinetic energy and ε the rate of dissipation. The k and ε equations, each contains nonlinear production and destruction source terms, which can be very large near the solid boundaries. According to linear stability theory, such terms can also severely reduce convergence rates if a purely explicit scheme is used to discretise the equations. The above numerical discretisation and grid adaptation technique has been used by T. Kuribayashi et al [19] for numerical simulation of their experimental works.

Three dimensional hexahedral cells with adaptive grids are used for these computations. In this mesh, the cell-edge data structures are arranged in such a way that each cell contains six faces which are sequence in one to six and each face indicates two neighboring cells that are left cell and right cell providing all faces of a cell are arranged in a particular way by positions and coordinates in the mesh. The sequential six faces in Figure 1(i) are *abod, adhe, abfe, efgh, bogf, dogh.*
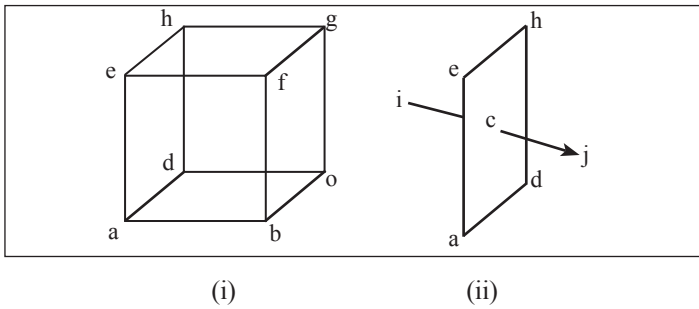
Figure 1: (i) Three-dimensional cell with six faces; (ii) Each face addresses the center of two neighboring cells, i and j

The grid adaptation is one of the improved and computational time saving techniques, which is used in these computations. The grid adaptation is performed by two procedures, one is refinement procedure and another is coarsening procedure. The refinement and coarsening operations are handled separately in computation. The criterion used for grid adaptation is based on the truncation error (ЄT) of the Taylor series expansion of density. The truncation error indicator ЄT is defined for every face of a cell and given by the ratio of the second-order derivative term to the first order one of the Taylor series of density so that

$$\epsilon_T = \max \left[\frac{|(\nabla\rho)_{lc} - (\nabla\rho)_i|}{(a_f\rho_c)/dl + |\nabla\rho|_i} \ , \ \frac{|(\nabla\rho)_{lc} - (\nabla\rho)_j|}{(a_f\rho_c)/dl + |\nabla\rho|_j} \right] \quad (8)$$

where *c* represent in Figure 1 (ii) the location of any face of a cell and *i* and *j* represent left cell and right cell of that face, *dl* is the center distance between cell *i* and *j*, $(\nabla\rho)_i$ and $(\nabla\rho)_j$ are the density gradient for cell *i* and *j*, $(\nabla\rho)lc = (\rho i - \rho j)/dl$, ρ_c is the density at the interface of right cell and left cell and α_f is the constant which is initially designed to prevent a zero denominator. In these computations, the value of αf is used 0.02 and it is problem-independent parameter. The refinement and coarsening operation for any cell depends on ϵ_T value and this ϵ_T value is determined for each face of a cell. The criterion for adaptation for any cell is

Refinement = maximum ϵ_T of six faces of a cell > ε_r

Coarsening = maximum ϵ_T of six faces of a cell < ε_c

where ε_r and ε_c are the threshold values for refinement and coarsening. In these computations, the values of ε_r are used 0.16~0.48 and the values of ε_c are used 0.12~0.44 and the higher values are used for higher shock Mach number. The level of refinement, used in all types of computation, is 2 or 3, depending on the number of cell per unit volume. The original 5 x 5 x 5 (mm) cell size will be 1.25 x 1.25 x 1.25 (mm) if refinement level is 2 and 0.625 x 0.625 x 0.625 (mm) if refinement level is 3.

In refinement procedure, the cells are selected for refinement in which every cell is divided into eight new sub cells and these new sub cells are arranged in a particular sequence so that these sub cells are used suitably in the data-structure. In threedimensional adaptation, the volume of new sub cells is 1/8 of primary cell where in two dimensional, this fraction is 1/4. To avoid unlimited cells refinement around shock waves, either the maximum level of refinement or the minimum cell volume or both are prescribed. When either the level or the volume of cell reaches the given limit, further refinement is prohibited. In the refinement procedure, it is required that no two neighboring cells differ by more than one refinement level. This one level-difference rule has accepted by many authors because it simplifies adaptation procedure and prevents pathologically large

volume ratios under certain circumstances. However, in unsteady calculations, the rule may be mismatch moving refined regions, say shock wave regions. To overcome this problem, pre-refinement is introduced. Once a cell cannot be refined due to the level difference between itself and one or a few neighboring cells, the neighboring cells are refined no matter what values of their refinement and coarsening are. In the coarsening procedure, the eight sub cells, which are generated from the primary cell, are restored into primary cell. The cell adaptive techniques are shown in Figures 2 (i) and (ii). The above three-dimensional adaptation strategy is based on an in-house 2-D solution adaptive code developed by Sun and Takayama [20].
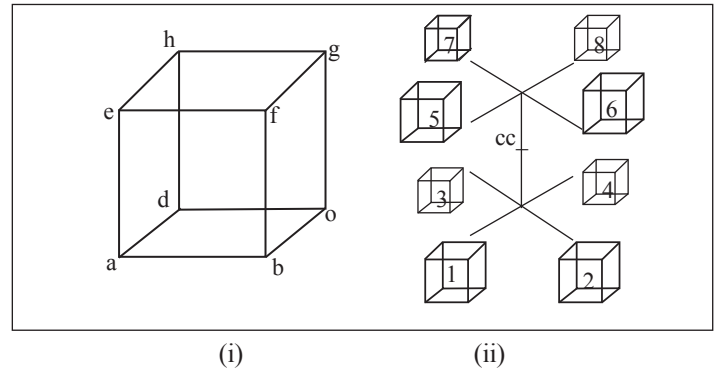

Figure 2: (i) Primary cell before adaptation where the center of the cell, cc is shown; (ii) Sequence of the eight cells after refinement of the primary cell as shown in Figure 2 (i)

## 4.0 TWO-DIMENSIONAL NUMERICAL VALIDATIONS

The experimental photographs, taken by double exposure holographic interferometry, are used for the code validation test and a comparison is conducted between experimental photographs and numerical images. The optical setup, present in the ISWRC laboratory, was used for the photographs and similar optical setup was also used by Sasoh *et. al.* [21] and other researchers in this laboratory. Many researchers conducted their code validation works on Navier-Stokes equations by using the flow over a flat plate. Some researchers used high-speed fluid flow around a cubic body to determine the velocity at different points on the axis of the cubic body and they attempted to simulate the viscous effect after determining the velocity along the axis numerically and experimentally.

In the present validation works, a visualisation technique is applied for the visualisation of the nozzle flow. For the purpose of code validation test, the shock wave propagation through a nozzle of small throat area is selected where laminar flow structures, transition phenomena, flow separation line as well as viscous boundary layer separation, wave propagation through the throat of the nozzle and shock wave reflection from converging area of the nozzle are observed numerically. The numerical code is used to solve the two-dimensional Navier-Stokes equations for the solution of the shock wave propagation through the nozzle and this code later has been extended to develop a three-dimensional code. The diameter of the throat of the nozzle is 2 mm and the details of the dimensions of the nozzle are shown in Figure 3 (i). The initial total number of cell is 10240 and the level of refinement is 3. All solid walls of the nozzle are taken as viscous solid wall boundary.

The upstream of incident shock wave is set as an inflow boundary condition, the properties and velocities of which are

calculated from Rankine-Hugoniot conditions with incident shock Mach number. Shock wave propagations through nozzle are studied experimentally and numerically for the incident shock Mach number 1.60. The numerical results, shown in Figures 3 and 7 are compared with the experimental results, shown in Figures 4, 6 and 8. Discussions on agreement/disagreement between experimental and numerical results are described below:
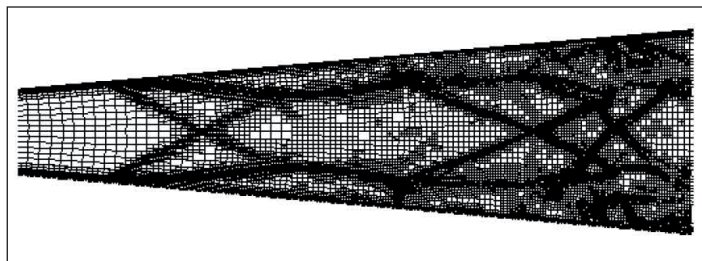
(a) An agreement is observed in the laminar part of this flow field, which is shown in Figures 3 to 8.
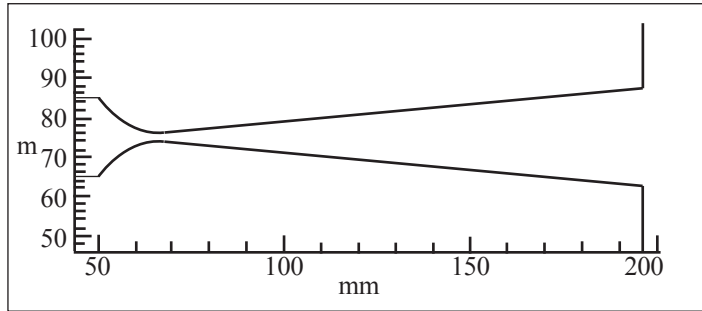
(i)
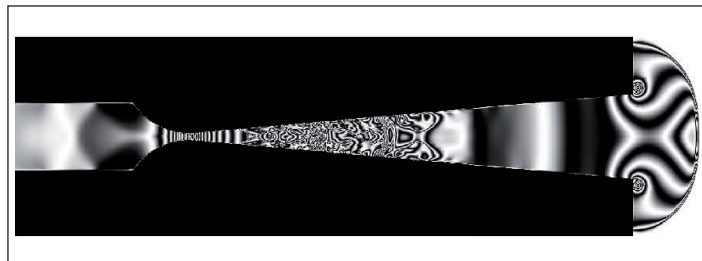
(ii)

(iii)

Figure 3: (i) Physical dimensions of the nozzle used in both experimental works; Numerical results (ii) Numerical density fringes at the time instant 28 millisecond; (iii) Corresponding adaptive grids in which point of separation, slipstream and boundary layer separation line are visible clearly

(b) At the moment of flow separation, the point of separation and the separation line, shown in the numerical results in Figures 3, 5 and 7, have some agreements with the experimental results in Figures 4, 6 and 8. It is observed that the flow separation is clearly appeared in Figure 3 (iii) and Figure 5 (ii) where high-level refinement is observed along the separation line.

(c) Wave propagation through the throat of the nozzle, shown in experimental results, has the good agreement with numerical results.

(d) Boundary layer in different location of the flow field appears both in the experimental and numerical results and a good agreement is observed in both results. In gird adaptation, it

is observed that the boundary layer separation line is clearly appeared in Figure 3 (iii) and Figure 5 (ii) where high-level refinement is observed along the boundary layer separation line.

(e) After the flow separation, an unsteady flow field appears and the flow transition period begins. In the transition period, some disagreement is observed between experimental results and numerical results. It may happen due to flow separation.
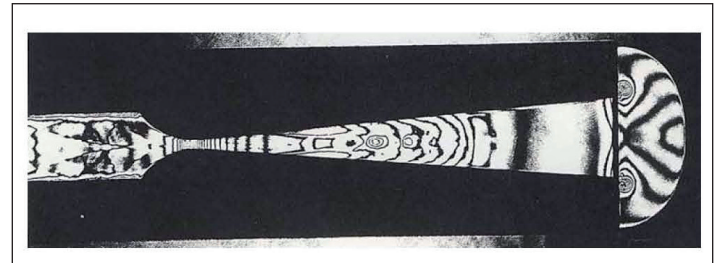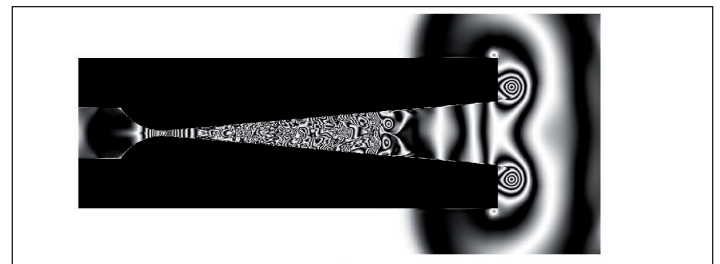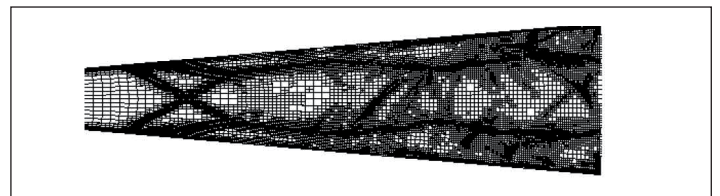

Figure 4: Experimental photo, taken by double exposure holographic interferometry; a shock wave propagating through nozzle at the same time instant 28 millisecond for viscous flow where the model of the nozzle is as Figure 3

(i)

(ii)

Figure 5: Numerical results (i) Numerical density fringes at the time instant 51 millisecond; (ii) Corresponding adaptive grids in which point of separation, slipstream and boundary layer separation line are visible clearly
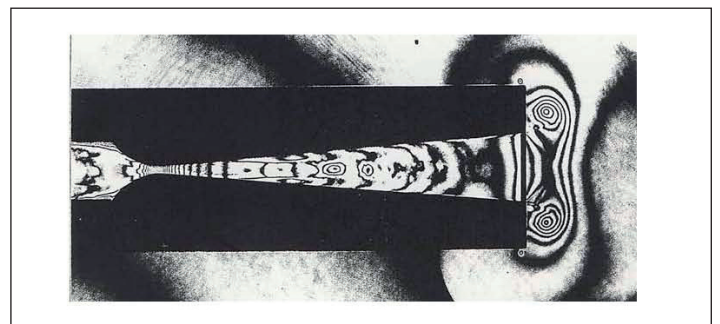

Figure 6: Experimental photo, taken by double exposure holographic interferometry; a shock wave propagating through nozzle at the same time instant 51 millisecond for viscous flow where the model of the nozzle is as Figure 3
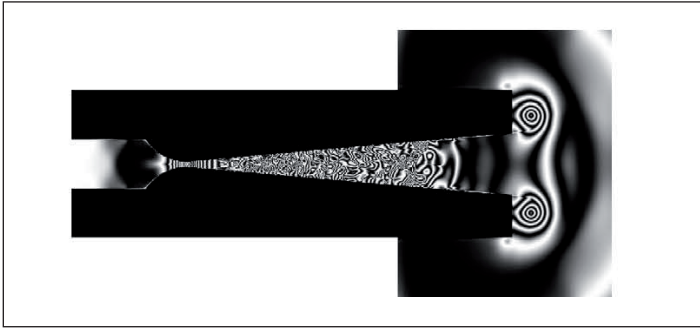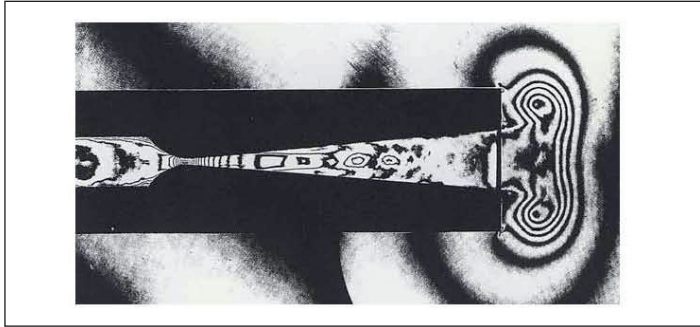
Figure 7: Numerical result: Numerical density fringes at the time instant 72 millisecond

Figure 8: Experimental photo, taken by double exposure holographic interferometry; a shock wave propagating through nozzle at the same time instant 72 millisecond for viscous flow where the model of the nozzle is as Figure 3

5.0 THREE-DIMENSIONAL NUMERICAL VALIDATIONS

5.1 Problem specifications

For the purpose of three-dimensional numerical code validations, the three-dimensional mesh with turbulence-generating grids is used, which is shown in Figures 9 (i), (ii). The physical size of each cell before adaptation is 5 x 5 x 5 (mm) and the initial number of cell is 1985. The adaptive grids and the selected turbulent region are shown in Figure 10, which are the two-dimensional sectional view of ZX-plane. The distance between the turbulence-generating grid and the end wall is 65 mm and in this distance, a turbulent region is selected so that there have no boundary effects in the turbulent region. The longitudinal distances (X/m) of any point on the centerline of the turbulent region are determined from turbulence-generating gird where m is the maximum dimensional length of a grid in the grid system. The distance, X = 0.0 mm at the position of turbulencegenerating grids. The value X/m = 3.776 is the starting point of the centerline of turbulent region and the value X/m = 11.376 is the ending point of the centerline of turbulent region. All turbulence parameters are measured before and after the shock or turbulence interaction in the selected turbulent region. In these computations, the threshold values for refinement are used 0.16~0.20 and the threshold values for coarsening are used 0.12~0.16 and the level of refinement is 2. Based on characteristic values, Reynolds number is 21546 and Prandtl number is 0.722.
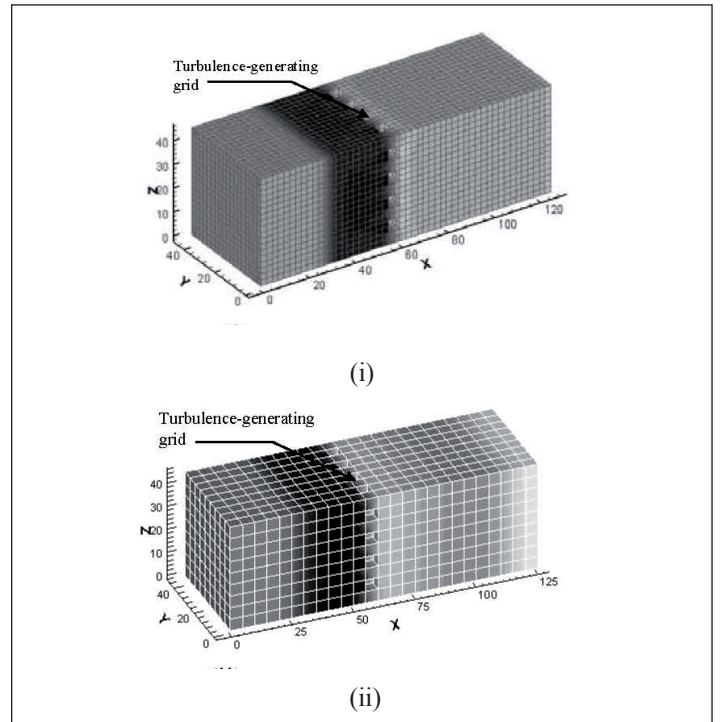

Figure 9: Three dimensional mesh and the position of the turbulence-generating grid plate are shown where different grid sizes are (i) $2 \times 2 \times 2$ grids/cm³; (ii) $4 \times 4 \times 4$ grids/cm³
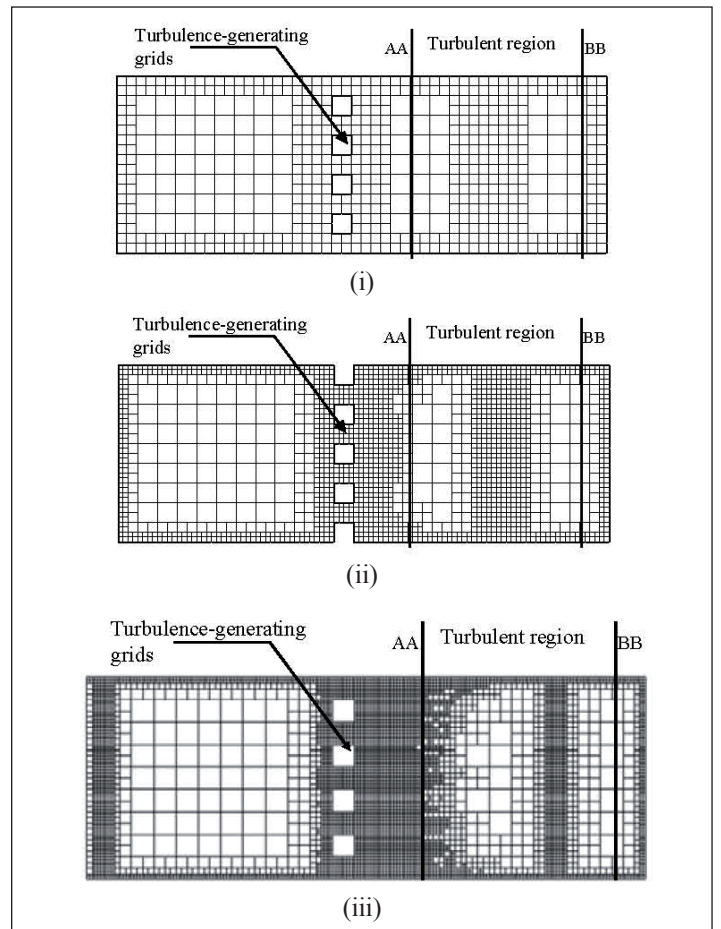

Figure 10: Two-dimensional cuts of the three-dimensional adaptive grids: (i) Level one; (ii) Level two; (iii) Level three

5.2 Grid convergence study

5.2.1 Using different level of refined grids

The study of the grid convergence on the present computational results has been carried out for different levels of grid refinement and for different grid sizes. The results, obtained for incident shock Mach number 1.50 are used for the study of the grid convergence. The refinement level one is used to solve the flow field with coarse grid and the refinement level three is used to solve the flow field with very refined grid. The results, obtained for level one, level two and level three refined grids, are compared with each other to observe the accuracy level of the computational results and such comparisons are used to determine the convergence behavior of the present simulation results. The two-dimensional sectional views of adaptive grids of level one, level two and level three refinements are shown in Figures10 (i), (ii) and (iii).

The grid size for refinement level one is 2.5 x 2.5 x 2.5 (mm), the grid size for refinement level two is 1.25 x 1.25 x 1.25 (mm) and the grid size for refinement level three is 0.625 x 0.625 x 0.625 (mm). The RMS (Root Mean Square) value of longitudinal velocity fluctuations or the longitudinal turbulence intensity, $<u>/U$ are determined along the centerline of the turbulent region for the different levels of refined grids which is shown in Figure 11.

It is observed that the longitudinal turbulence intensity profile, obtained from the refinement level one, has some deviations with the profiles for higher refinement level and the longitudinal turbulence intensity profile for the refinement level two has the good agreement with the longitudinal turbulence intensity profile for the refinement level three and some disagreements are observed at the position near the turbulence grids. Similarly the lateral velocity fluctuations, $v´/U$ and $w´/U$ are determined along the centerline of the turbulent region for the different levels of refined grids and it is observed that there have the good agreements between the lateral velocity fluctuations profiles, obtained for higher level of refined grids. Figure 12 shows the average pressure variations across the reflected shock wave for the different levels of refined grids. It is observed that there have the good agreements between the average pressure profiles across the shock wave, obtained for higher level of refined grids.

5.2.2 Using different grid sizes

The utilities of the grid refinement in grid convergence study are sometimes difficult if there have the more deviations between the results obtained by two successive levels of the grid refinement. In that case different sizes of the grid are suitable to use for grid convergence study. Different grid sizes are 2 x 2 x 2 grid and 4 x 4 x 4 grid per cubic centimeter. For the size of 2 x 2 x 2 grid, the initial number of grid in the computational domain is 1985 and the computational domain is shown in Figure 9 (i). Similarly for the size of 4 x 4 x 4 grid, the initial number of grid in the computational domain is 15880 and the computational domain is shown in Figure 9 (ii). So, it is observed that different turbulent parameters in the turbulent region are determined for different number and size of the grids contain in the turbulent region.

The lateral planes intersect the centerline of the turbulent region, are used to determine different turbulent parameters. Each lateral plane contains several grids and the number of grid depends on the number of grid per unit volume in the turbulent region. For 4 x 4 x 4 grid, the number of grid in the lateral plane is approximately four times more than for 2 x 2 x 2 grid.

The computational results for different grid sizes are compared and performed the independence test of grid size in the present simulation results. All the results, obtained before and after the shock/turbulence interaction, are used to determine the independence test of grid size. The longitudinal turbulence intensity, $<u>/U$ are determined along the centerline of the turbulent region for different grid sizes of 2 x 2 x 2 grid and 4 x 4 x 4 grid and the comparison between the characteristic profiles of the longitudinal turbulence intensity for different grid sizes are shown in Figure 13. It is observed in Figure 13 that the characteristic profiles for different grid sizes are simulated each other and the result indicates the independency on grid size in the present computations. Similarly the lateral velocity fluctuations, $v´/U$ and $w´/U$ are determined along the centerline of the turbulent region for different grid sizes of 2 x 2 x 2 grid and 4 x 4 x 4 grid and it is observed that the characteristic profiles of lateral velocity fluctuations for different grid sizes are simulated each other and the simulation results are independent on the grid size.

The normalised average pressure variations are determined across the reflected shock wave for different grid sizes of 2 x 2 x 2 grid and 4 x 4 x 4 grid and the comparison between the average pressure profiles for different grid sizes are shown in Figure 14. It is observed in Figure 14 that the average pressure profiles across the shock wave for different grid sizes are simulated each other and this result also indicates the independency on grid size in the present computations.
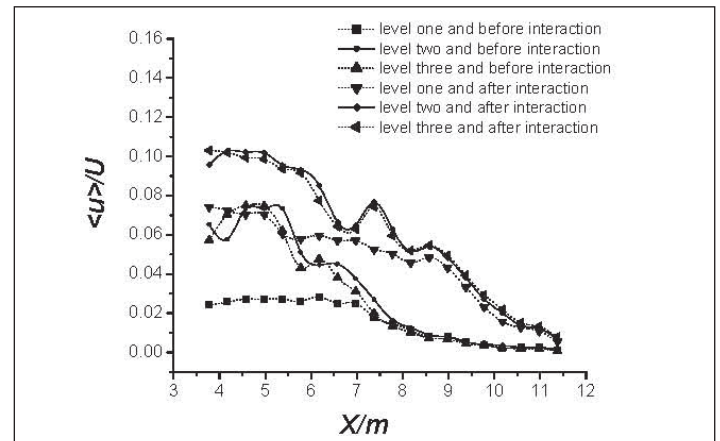

Figure 11: Longitudinal turbulence intensity ($<u>/U$) before and after the shock/turbulence interaction along the centerline of the turbulent region for different grid refinement levels

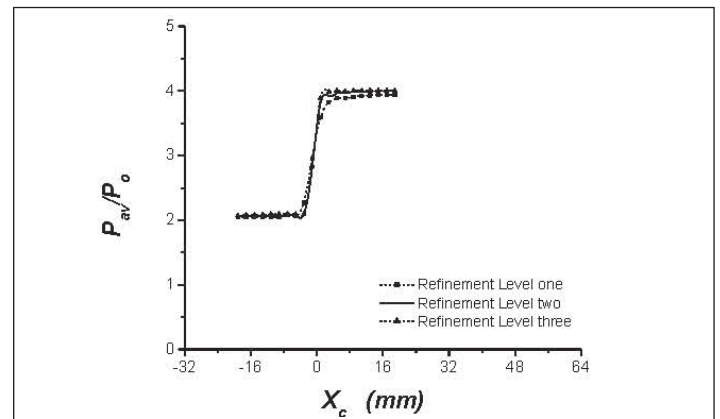*Figure 12: Average pressure (Pav/Po) variations across the reflected shock wave for different grid refinement levels, where the origin, Xc=0.0 corresponds to the shock location and X/m =7.6*
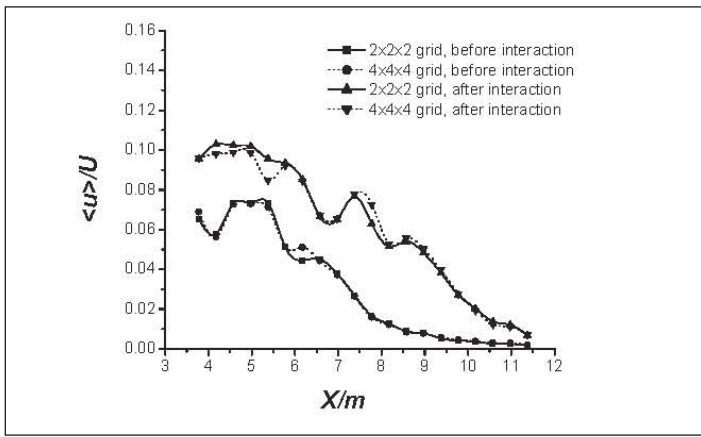
Figure 13: Longitudinal turbulence intensity (<u>/U) before and after the shock/turbulence interaction along the centerline of the turbulent region for different grid sizes
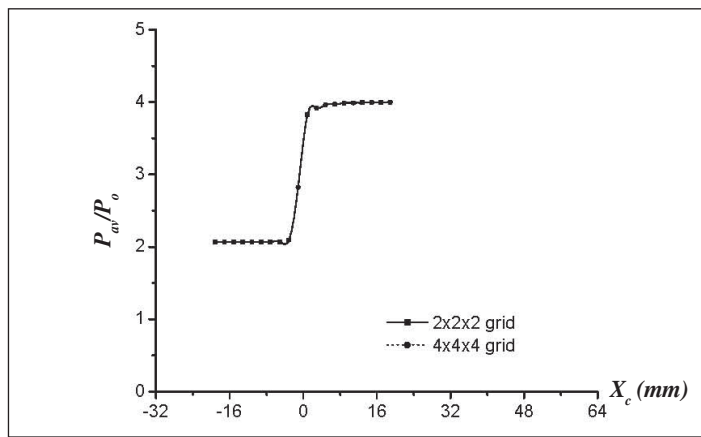

Figure 14: Average pressure (P_{av}/P_o) variations across the reflected shock wave for different grid sizes, where the origin, $X_c = 0.0$ corresponds to the shock location and X/m = 7.6
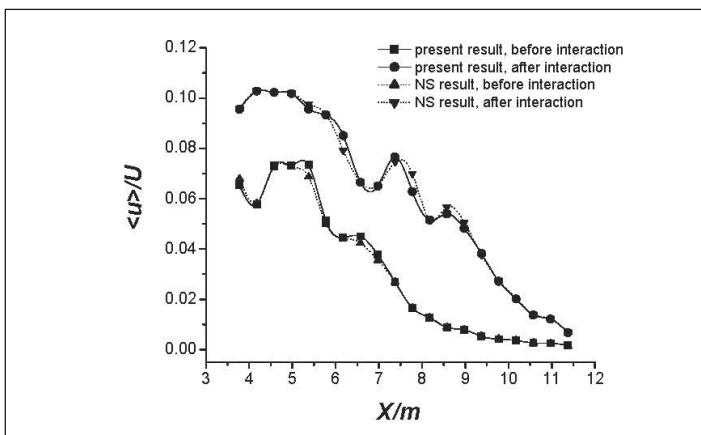

Figure 15: Comparison between the present simulation results and the NS results for the longitudinal turbulence intensity (<u>/U) along the centerline of the turbulent region before and after the shock/turbulence interaction

5.3 Comparison with the Navier-Stokes simulation (NS) results

For the purpose of the numerical code validation test, the present simulation results are compared with the Navier-Stokes simulation (NS) results and the results, obtained for shock Mach number 1.50, are used for this comparison. The comparison results

indicate that the present threedimensional code with turbulence model is working very well for the present flow conditions. The turbulence model is used to solve some turbulence parameters directly and these turbulence parameters are used to determine the interaction effects properly. Navier-Stokes simulation (NS) is also performed for the shock or turbulence interaction with $M_s = 1.50$ where shock wave is captured. The solution of the Navier-Stokes equations is used to compare with the present simulation results and the present simulation results have the good agreements with the NS results.

The longitudinal turbulence intensity, $<u>/U$ before interaction and after interaction are characterised along the centerline of the turbulent region which is shown in Figure 15. The characteristic behaviors of the RMS value of longitudinal velocity fluctuations along the centerline of the turbulent region have the good agreements with the NS results and these agreements validate the present simulation results. The amplification of turbulent intensity and the amplification of turbulent kinetic energy level are determined for the shock wave interaction with turbulent field and these results are compared with the NS results, which are shown in Table 1.

Table-1: Comparison between the present simulation results and the NS results

Amplifications of	Incident shock Mach number	(Present simulation results)	(NS results)
Turbulent intensity	1.50	1.98~2.12	2.02~2.16
TKE level	1.50	3.08~3.41	3.20~3.55

Similarly the lateral velocity fluctuations, v'/U and w'/U are characterised along the centerline of the turbulent region and it is observed that the present computational results for the lateral velocity fluctuations, v'/U and w'/U have the good agreements with the NS results. The normalised pressure fluctuations characteristic curves before interaction and after interaction along the centerline of the turbulent region and it are shown that no substantial amplification of the pressure fluctuations occurs after interaction and it has good agreement with the NS results. The normalised average pressure, P_{av}/P_o variations are characterized across the reflected shock wave when the position of the reflected shock wave is in the turbulent region, which is shown in Figure 16 and the pressure profile obeys the shock reflection theory and also has the good agreement with the NS results. Even though all pressure values are not suitable for code validation but these are carrying good information about the characteristics of the selected turbulent region in the wake of the turbulence grid.

The solution of Navier-Stokes equations provides the information of turbulent kinetic energy (TKE) level in the flow field where the TKE is computed from the equation, $1/2 (u'^2 + v'^2 + w'^2)$ and in this case, the values of TKE are directly related to the velocity fluctuations of the fluid particles. On the other hand, the TKE is obtained from the solution of two equations of k-ε turbulence model and the accuracy of the TKE value depends on the modeling equations. The values of TKE obtained from

the velocity fluctuations of the fluid particles in the flow field are necessary to compare with the values of TKE obtained from the solution of two equations of $k\text{-}\varepsilon$ turbulence model because all turbulence modeling equations are not ideal and it must have some deviations between these results. The comparisons between the TKE values obtained from the solution of Navier-Stokes equations and the solution of turbulence model are determined along the centerline of the turbulent region for $M_s = 1.50$ and the comparisons are shown in Figure 17. Using the equation, $1/2\ (u'^2 + v'^2 + w'^2)$, Rotman (1991) computed the TKE level in the flow field and it was observed that the maximum amplification factor of TKE level was 2.00 in the two dimensional computational results inside the Mach number range 1.01-1.50. The amplification of TKE level obtained from the velocity fluctuations is compared with the amplification obtained from the solution of turbulence model, which is shown in Figure 18, and it is observed in Figure 18 that the deviations between these results are 10 to 20 %.
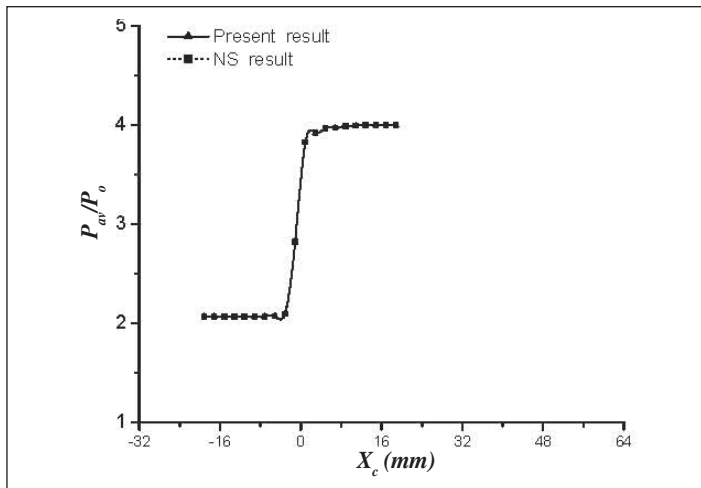

Figure 18: Comparison between the amplification of turbulent kinetic energy level obtained from the velocity fluctuations and the turbulence model

6.0 CONCLUSIONS

A good numerical simulation for nozzle flow depends on the throat area and the converging or diverging angle of the nozzle and the strength of the shock wave propagate through the throat of the nozzle. For small throat area of the nozzle, the flow separation will be high and blockage ratio will be low. In that case, it is necessary to select the shock wave strength comparatively high for good numerical simulations. So it is found that numerical results for higher shock Mach number have the good agreement with experimental results. Other flow parameters like fluid viscosity, Reynolds number also effect on the simulation results.

After the validation test of the Navier-Stokes equations, the extended three-dimensional Navier-Stokes equations with $k\text{-}\varepsilon$ turbulence model are developed to solve almost all types of shock or turbulence interaction problems. Even though such type of computations is complex to get proper solution, but maximum simulated data agrees with the experimental results, performed by other researchers. In these computations, three-dimensional adaptive grids are used to get more accurate solution. Due to grid adaptation, the number of new cell, generated after refining operation, is twice the number of new cell, generated in two-dimensional adaptation and also adaptation is happened in the direction of the three Cartesian Coordinates. So the total number of cell difference between two subsequent refinement levels increases sharply, as a result, increases the computational time. The advantage of three-dimensional code is to solve all the turbulent parameters in the three-dimensional space system because the shock or turbulence interaction effect is one of the three-dimensional problems. The study of the grid convergence test has been performed successfully with different levels of grid refinement and also with different sizes of the grid. It is observed that all the simulation results are completely independent of the present grid system. The comparisons between the present simulation results and the NS results have been conducted successfully and it is observed that there have the good agreements between the present simulation results and the NS results. ■

Figure 16: Comparison between the present simulation results and the NS results for the normalised average pressure (P_{av}/P_o) variation across the shock wave when the position of the shock wave is in the turbulent region and where the origin, $X_c = 0.0$ corresponds to the shock location and X/m = 7.6
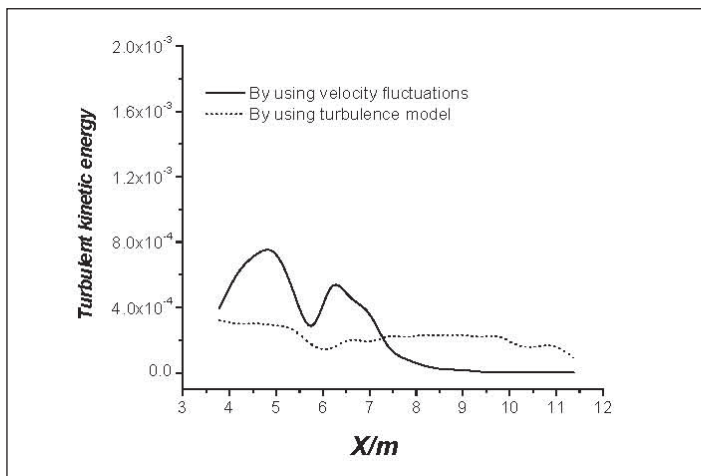

Figure 17: Comparison between the values of turbulent kinetic energy along the centerline of the turbulent region obtained from the velocity fluctuations and the turbulence model
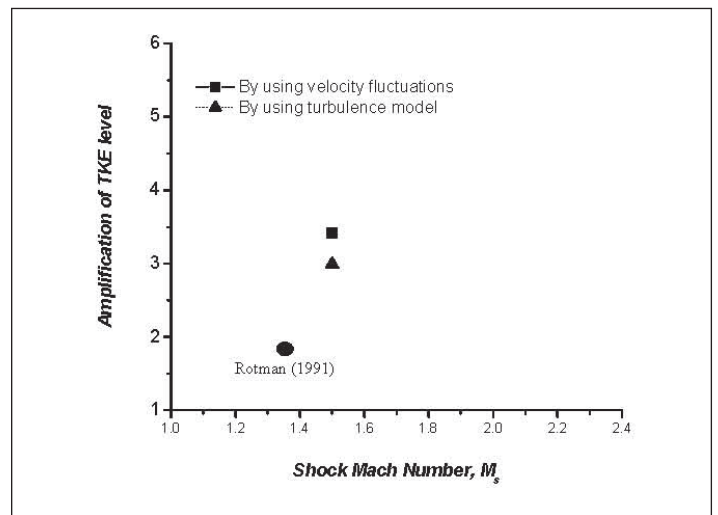
REFERENCES

[1] Ribner HS. (1953) Convection of a pattern of vorticity through a shock wave, NACA TN-2864.

[2] Ribner HS. (1954) Shock-turbulence interaction and the generation of noise, NACA TN-3255.

[3] Ribner HS. (1969) Acoustic energy flux from shock-turbulence interaction, Journal of Fluid Mechanics 35: pp. 299-310.

[4] Kovasznay LSG. (1953) Turbulence in supersonic flow, Journal of the Aeronautical Science 20: pp. 657-682.

[5] Lighthill MJ. (1953) On the energy scattered from the interaction of turbulence with sound or shock waves. Proc. Camb. Phil. Soc, 49: pp. 531-551.

[6] Moore FK. (1953) Unsteady oblique interaction of a shock wave with a plane disturbances, NACA TN-2879.

[7] Kerrebrock JL. (1956) The interaction of flow discontinuities with small disturbances in a compressible fluid. Ph.D. thesis, California Institute of Technology.

[8] Ribner HS. (1987) Spectra of noise and amplified turbulence emanating from shock-turbulence interaction. AIAA J. 25: pp. 436-442.

[9] Anyiwo JC and Bushnell DM. (1982) Turbulence amplification in shock-wave boundary-layer interaction, AIAA J. 20: pp. 893-899.

[10] Sekundov AN. Supersonic flow turbulence and interaction with a shock wave, Izv. Akad. Nauk SSR Mekh. Zhidk. Gaza, March-April 1974.

[11] Donsanjh DS, (1964) Weeks TM. Interaction of a starting vortex as well as Karman vortex streets with traveling shock wave, AIAA paper No. 64-425.

[12] Chu BT and Kovasznay LSG. (1957) Non-linear interactions in a viscous heat- conducting compressible flow, Journal of Fluid Mechanics 3: p. 494.

[13] Devieve JF and Lacharme JP. (1986) A shock wave/ free turbulence interaction. Turbulent shear layer/shock wave interaction, edited by J. Delery, Springer-Verlag, Berlin.

[14] Jacquin L, Blin E and Geffroy P. (1991) Experiments of free turbulence/shock wave interaction, Proc. Turbulent shear flows, 8, tech Univ, Munich, Ger. p. 1-2-1-1-2-6.

[15] Debieve FR, Gouin H and Gaviglio J. (1982) Momentum and temperature fluxes in a shock wave-turbulence interaction. In Structure of Turbulence in heat and mass Transfer (ed. Z. P.Zaric). Hamisphere.

[16] Hesselink L and Sturtevant B. (1988) Propagation of weak shocks through a random medium, J. Fluid Mechanics 196: pp. 513-553.

[17] Richtmyer RD, (1960) Taylor instability in a shock acceleration of compressible fluids, Communications on Pure and Applied Mathematics 13: pp. 297-319.

[18] Meshkov EE. Izv. Akad. (1969) Instability of the interface of two gases accelerated by ashock wave, Nauk SSSR Mekh. Zhidk. Gaza 4: 151.

[19] Kuribayashi T.,Ohtani K., Takayama K., Menezes V., Sun M. and Saito T. (2007) Heat flux measurement over a cone in a shock tube flow, Shock Waves 16: pp. 275-285.

[20] Sun M and Takayama K (1999) Conservative smoothing on an adaptive quadrilateral grid, Journal of Computational Physics 150: pp. 143-18.

[21] Sasoh A., Matsuoka K., Nakashio K., Timofeev E., Takayama K., Voinovich P., Saito T., Hirano S., Ono S. and Makino Y. (1998) Attenuation of weak shock waves along pseudoperforated walls, Shock Waves 8: pp. 149-159.

PROFILES

ASSOC. PROF. DR MOHAMMAD ALI JINNAH is an Associate Professor in Department of Mechanical and Chemical Engineering, Islamic University of Technology (IUT) (An Organ of the OIC), Bangladesh. He obtained his Ph.D. from Tohoku University, Sendai, Japan in 2005 spesialising in Shock Wave interaction with turbulent flow. Het got his B. Sc Engineering (Mechanical) in 1993 and M.Sc. Engineering (Mechanical) in 18998 from BUET, Dhaka. He joined as an Assistant Engineer in Titas Gas T&D Company and served up to 2001. After getting his Ph.D, he joined as an Assistant Professor in IUT and is working stilll now.

EMERITUS PROF. KAZUYOSHI TAKAYAMA obtained his doctoral degree from Tohoku University in 1970 and was then appointed lecturer at the Institute of High Speed Mechanics, Tohoku University, promoted to Associate Professor in 1975 and to professor in 1986. He was appointed Director of the Shock Wave Research Center at the Institute of High Speed Mechanics in 1988. The Institute of High Speed Mechanics was restructured as the Institute of Fluid Science in 1989. He retired in 2004 and became Emeritus Professor of Tohoku University. In 1990 he launched Shock Waves, an international journal, taking on the role of managing editor and in 2002 became editor-in-chief. He was elected president of the Japan Society for Aeronautical and Space Sciences for one year in 2000 and was chairman of the Japanese Society of Shock Wave Research in 2000. He was appointed president of the International Shock Wave Institute in 2005. His research interests range from fundamental shock wave studies to the interdisciplinary application of shock wave research.